Climate Dynamics (2022) 59:3069–3086
https://doi.org/10.1007/s00382-022-06240-1

Extreme austral winter precipitation events over the South-American Altiplano: regional atmospheric features

Hans Segura[1,2] · Jhan Carlo Espinoza[1] · Clementine Junquas[1] · Thierry Lebel[1] · Mathias Vuille[3] · Thomas Condom[1]

Received: 29 May 2020 / Accepted: 2 March 2022 / Published online: 4 April 2022

Abstract

The South American Altiplano has a marked dry season during the austral winter (June to August, JJA). However, during this season synoptic meteorological conditions triggering heavy precipitation can damage socioeconomic activities, often causing the loss of human lives. Using daily in-situ precipitation data from 39 rain-gauge stations over the northern Altiplano (18°S -15°S; > 3000 m.a.s.l.) for the JJA season, we computed the historical percentile 90 (p90) and we identified extreme rainy days with precipitation higher than p90 in the 1980–2010 period. We identified 100 winter extreme precipitation events (WEPEs) over this region that can last between one to 16 days. The K-means analysis was applied to anomalies of geopotential height at 500 hPa from ERA-Interim data during the initial day or Day(0) of WEPEs lasting 1 day (42 cases), 2 days (19) and more than 2 days (39). We found 59 WEPEs characterized by an upper-level trough over the Peruvian-Chilean coast. At 850 hPa, these 59 WEPEs are also associated with cold surges along the eastern Central Andes, indicating an association between the upper-level trough and the cold surge in developing deep convection over the northern Altiplano. A lead-lag composite analysis further showed a significant lower- and mid-tropospheric moistening over the western Amazon 2 days before the onset of these 59 WEPEs, due to low-level northerly wind anomalies originating over equatorial South America. The other 41 WEPEs are associated with a low-level southerly wind regime crossing the equator and a mid-and upper-level low-pressure system over the Peruvian-Chilean coast. While the low-level southerly regime enhances mid-tropospheric moisture transport from the equator towards the Altiplano due to the developed shallow meridional circulation when propagating equatorward, a low-pressure system promotes intensification of upward motion, boosting the upslope moisture transport from the lowlands to the east of the Central Andes towards the Altiplano.

Keywords Winter extreme precipitation · Altiplano · Cold surges · Upper-level trough · Amazon convection

1 Introduction

The Central Andes, located between 15 °S and 25 °S, are geographically bound by the Amazon to the east and the eastern tropical Pacific to the west. The interaction between the orography and the atmospheric circulation modulates the spatial pattern of precipitation in the Central Andes, characterized by an east–west gradient, with wet regions near the Amazon border (e.g. Bendix and Lauer 1992; Houston and Hartley 2003; Garreaud 2009; Espinoza et al. 2015). The Altiplano is an arid region located in the upper-elevation zones of the Central Andes above 3000 m.a.s.l., where the annual precipitation value is approximately between 200 and 700 mm year^{-1} (Garreaud et al. 2003; Vuille and Keimig 2004). Indeed, between 50 and 75% of the annual precipitation over the Altiplano falls during austral summer (December–February), associated with the development of the Bolivian High and convection over the western Amazon (e.g. Lenters and Cook 1997, 1999; Garreaud 1999b; Vuille 1999; Espinoza et al. 2020; Segura et al. 2020). On the other hand, the contribution of austral winter precipitation to the annual amount is small in the Altiplano, but extreme precipitation events during this season, including rain, snow and hailstorms, have strong social and

✉ Hans Segura
hans.msc90@gmail.com

1 University of Grenoble Alpes, IRD, CNRS, Grenoble INP, IGE, 38000 Grenoble, France

2 Max Planck Institute for Meteorology, Bundestrasse 53, 20146 Hamburg, Germany

3 Department of Atmospheric and Environmental Sciences, State University of New York at Albany, Albany, New York, USA

economic impacts on Andean societies (Poveda et al. 2020; Imfeld et al. 2021). Indeed, these events cause considerable damage to road infrastructure, crop fields, and the livestock sector as well as being responsible for the loss of human lives (Sistema Nacional de Defensa Civil 2006; Perea-Flores 2018). Thus, the objective of this study is to understand the atmospheric mechanisms associated with austral winter (June–July–August; JJA) extreme precipitation events in the northern Altiplano, a region located in the Central Andes between 18 °S and 15 °S, above 3000 m.a.s.l.

During austral winter, the retreat of the South American Monsoon System (SAMS) reduces the development of deep convection over most of the southern part of tropical South America, and as a consequence, upper-level easterlies do not exist over this region (e.g. Silva Dias et al. 1983; Horel et al. 1989; Lenters and Cook 1997; Zhou and Lau 1998; Wang and Fu 2002; Vera et al. 2006; Garreaud et al. 2009; Nie et al. 2010). Therefore, mid- and upper-level westerlies originating over the cold and dry eastern tropical Pacific prevail over the central Andes during JJA (Garreaud 1999b; Vuille 1999; Garreaud 2009; Espinoza et al. 2020). Mid- and upper-level westerlies introduce westerly momentum flux over the eastern Andean ridge, thereby preventing the upslope transport of moist air from the western Amazon toward the Altiplano (Garreaud 1999b). Another important mechanism for inhibiting precipitation on the Altiplano is the large-scale subsidence associated with the regional Hadley Cell due to the convection over northern South America (Wang and Fu 2002; Vera et al. 2006; Garreaud et al. 2009; Espinoza et al. 2021). Thus, this explains the small amount of precipitation over the Altiplano during austral winter. Notwithstanding this atmospheric circulation, the Altiplano has faced extreme precipitation events during this season (Vuille and Ammann 1997; Poveda et al. 2020; Imfeld et al. 2021).

Cold air incursions, also called "cold surges", originating in mid-latitudes over South America are one among several synoptic-scale circulations influencing extreme precipitation events over the eastern Central Andes (Garreaud and Wallace 1998; Garreaud 1999a; Boers et al. 2015; Hurley et al. 2015; Eghdami and Barros 2019; Poveda et al. 2020; Imfeld et al. 2021). Indeed, cold surge events are a distinctive feature of the South American climatology, and they are observed in all seasons (Garreaud and Wallace 1998; Garreaud 2000; Vera and Vigliarolo 2000; Alvarez et al. 2013; Espinoza et al. 2013; Paccini et al. 2018). Garreaud (2000) showed that the precursor of cold surges consists of a cold high-pressure system at lower-levels, originating over the subtropical eastern Pacific and crossing the Andes between 30 °S and 45 °S to reach southern Argentina (see Figure 10 in Garreaud 2000). At this point of the event, the low-level flow is geostrophic, but the blocking effect of the subtropical Andes turns the low-level flow into an ageostrophic, terrain-parallel flow, with a northward direction that allows the incursion to propagate into lower latitudes. Occasionally, these cold surges can reach the equatorial regions of South America (Parmenter 1976; Marengo et al. 1997; Garreaud 1999a, 2000; Vera and Vigliarolo 2000; Seluchi et al. 2006; Bowerman et al. 2017; Figueroa et al. 2020). It is important to signal that cold surges could also be part of the interaction between convection in the equatorial region of South America and the extratropics as explained by Kasahara and da Silva Dias (1986).

During the austral summer, the convergence of low-level southerlies with warm and moist low-level northerlies originating over the Amazon creates a NW-SE oriented band of strong precipitation, extending from the eastern Central Andes toward the Atlantic, reflecting the leading edge of the cold surge (see Figure 3 in Garreaud and Wallace 1998; Garreaud 1999a, 2000). It is important to note that the NW–SE orientation of the rainfall band is also influenced by the Andes' topography, and the heat source over the Amazon basin and Central Brazil helps sustains the NW–SE oriented low-level convergence zone (Figueroa et al. 1995). Along the eastern slopes of the Central Andes, precipitation occurs at the intersection of the cold surge with the terrain (1000–2000 m.a.s.l) which is also the altitude of maximum moisture flux during cold surge events (Chavez and Takahashi 2017; Eghdami and Barros 2019). In the northeastern Altiplano, Hurley et al. (2015) showed that cold surges trigger extreme precipitation during the austral summer, and they are responsible for most of the snowfall at Quelccaya Ice Cap in Peru (70.82 °W, 13.93 °S; 5670 m.a.s.l.). In the austral winter, cold surge events trigger the same dynamic response in tropical South America, with a NW–SE oriented band of precipitation extending from the central Amazon towards the Atlantic coast (Garreaud 2000; Espinoza et al. 2013; Bowerman et al. 2017; Paccini et al. 2018). In addition, the better defined NW–SE oriented band of precipitation in this season could be explained by the basic state of the Southern Hemisphere winter, in particular due vertical and meridional shear of the zonal wind (Kasahara and da Silva Dias 1986).

While cold surges have also been related to cloud cover over the Altiplano (Sicart et al. 2016), the relationship between extreme precipitation events over the Altiplano and cold surge events during austral winter has not been explored in detail. Sicart et al. (2016) used in-situ meteorological data to calculate a cloud index (CI) at Zongo Glacier (16 °S, 5050 m.a.s.l.). The authors showed that about 87% of the highest values of CI (extreme cloudy days) during JJA are, indeed, related to cold surge events that reach the Bolivian Andes. The remaining 13% are associated with anomalous upper-level trough conditions over the Chilean coast at 45 °S. Upper-level troughs are characterized by low-pressure and cold air temperature anomalies between 500

and 200 hPa, but increased air temperature above 200 hPa due to tropopause folding (Hoskins et al. 1985; Cox et al. 1995; Kiladis 1998; Knippertz 2007). In addition, strong updrafts along the eastern side of the upper-level troughs can produce precipitation when approaching regions characterized by a moist and warm troposphere. Several studies have shown that upper-level troughs can develop into cut-off lows, which are isolated cells moving equatorward (Hoskins et al. 1985; Kiladis and Weickmann 1992; Knippertz and Martin 2005; Campetella and Possia 2006; Garreaud and Fuenzalida 2007; Pinheiro et al. 2017; Wernli and Sprenger 2007). Vuille and Ammann (1997) evidenced that snowfall during six dry seasons (May–September of 1984, 1986 and 1990–1993) over the south-central Altiplano (25 °S–20 °S) are mainly influenced by cut-off lows originating over the eastern Pacific. In a recent study, the passage of upper-level troughs over the Altiplano was identified as the principal factor triggering precipitation over the Peruvian Andes during austral winter (Bonshoms et al. 2020). However, the authors showed that dry synoptic conditions in the Peruvian Andes could equally be associated with the passage of upper-level troughs. Thus, it remains unclear if convection over the Altiplano is triggered by the presence of upper-level troughs alone, or if it requires an interaction of the upper-level trough with other atmospheric mechanisms. For instance, it could be that weakened convection over northern South America decreases subsidence over the Altiplano. Furthermore, how these circulation anomalies relate to extreme precipitation events over the northern Altiplano have not yet been explored.

Thus, the goal of this study is to identify the atmospheric mechanisms triggering extreme precipitation events over the dry northern Altiplano, a region where studies regarding winter extreme precipitation events are scant. Using in-situ precipitation data from the northern Altiplano, we characterize for the first time extreme precipitation events occurring in June to August (JJA) from 1980 to 2010. The ERA-Interim reanalysis data set (Dee et al. 2011) was used to map low-, mid- and upper-level atmospheric circulation over South America and the eastern Pacific at the onset of these extreme events. Likewise, we made use of the CHIRPS precipitation product (Funk et al. 2015) to detect regions in South America where rainfall could be associated with extreme precipitation events over the northern Altiplano.

This paper has the following structure. In Sect. 2 we present the data and the methodology of this study. Characteristics of the identified extreme precipitation events, including their duration and the associated atmospheric circulation at the onset of the events, are presented in Sect. 3. In Sect. 4, we present the two atmospheric configurations associated with heavy precipitation in the northern Altiplano, identified by using the K-means clustering analysis. Their associated precipitation and atmospheric circulation are described in Sects. 5 and 6. Finally, conclusions are presented in Sect. 7.

2 Data and methods

2.1 Data

2.1.1 In-situ precipitation data over the northern Altiplano

We made use of 39 rain-gauge stations, from the Peruvian and Bolivian meteorological services (SENAMHIs), located over the northern Altiplano (18 °S–15 °S; >3000 m.a.s.l.; Figure 1a; Table S1) collected by the project "Data on climate and Extreme weather from the Central Andes" (DECADE; Hunziker et al. 2017). Hunziker et al. (2017) stated that rain-gauge stations in the Altiplano present measurement problems. Typical measurement errors include truncation in the maximum value of precipitation, gaps, systematic missing values on specific days of the week, among others. Due to these measurement problems, Andrade (2018) chose those 39 rain-gauge stations in which measurement errors are minimal to analyze trends in extreme precipitation events for the 1980–2010 period. For further information on the tests applied to the 39 rain-gauge stations, see Hunziker et al. (2017). Thus, using the same 39 rain-gauge stations, we analyzed only daily precipitation in all austral winter seasons (JJA) for the period 1980–2010, meaning that 2852 days were used in this study. All days in austral winter for the 1980–2010 period have precipitation data from at least 27 rain-gauge stations, with most of the days having a maximum of 39 rain-gauge stations available (Figure S1a). In addition to these 39 stations, we also used 62 additional lower-quality rain-gauge stations located across the Altiplano only for composite analyses only (Fig. 1a, Table S1), allowing for a more thorough analysis of the spatial precipitation structure during extreme precipitation events in the Altiplano.

2.1.2 CHIRPS data set

The Climate Hazard group Infrared Precipitation with Station (CHIRPS) dataset is a gridded precipitation product resulting from the combination of satellite precipitation estimates and in-situ precipitation data (Funk et al. 2015). The high spatial resolution (0.05° × 0.05°) and its long temporal coverage (1982–2018) render CHIRPS one of the most useful precipitation products to study precipitation variability over the tropical Andes (Paccini et al. 2018; Sulca et al. 2018; Satgé et al. 2019; Segura et al. 2019, 2020). In this study, we use CHIRPS at a daily time scale during the austral winter seasons in the 1981–2010 period in order to identify regions over tropical

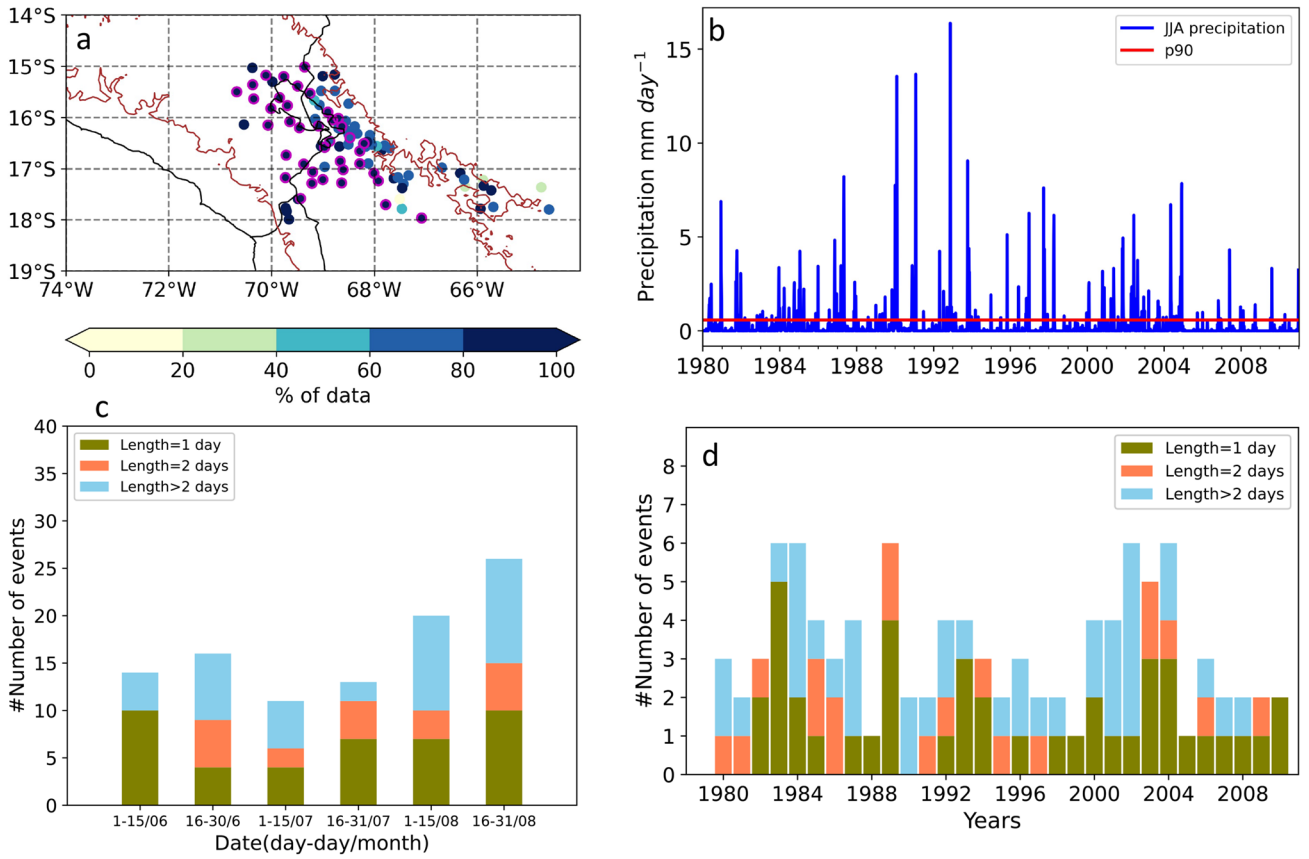

Fig. 1 **a** Percentage of days with data available at each rain-gauge station. The 39 rain-gauge stations used to calculate the winter extreme precipitation events in the Altiplano are marked by circles with magenta contour. The total number of days during June-August seasons in the 1980–2010 period is 2852. The red line denotes the altitude of 3000 m.a.s.l. **b** Daily precipitation time series of the northern Altiplano (PP-Andes) calculated by using the arithmetic mean from the 39 rain-gauge stations in magenta shown in **a**. The red horizontal line is the percentile 90 of PP-Andes. **c,d** Frequency of winter extreme precipitation events (WEPEs) as a function of 15-day intervals in each month (June-06; July-07; August-08) and year, respectively. In **c** and **d**, brown, orange and cyan bars represent WEPEs lasting 1 day, 2 days and more than 2 days, respectively

South America where precipitation is associated with extreme precipitation events over the northern Altiplano.

2.1.3 Atmospheric reanalysis data set

We used horizontal wind and vertical motion, temperature, specific humidity and geopotential height from the ERA-Interim reanalysis data set (http://apps.ecmwf.int/datasets/data/interim-full-daily/; Dee et al. 2011). The atmospheric variables have a spatial resolution of 0.5° × 0.5° and cover pressure levels from 1000 to 100 hPa. We analyzed these atmospheric variables at a daily time scale for the June-August season in the 1980–2010 period.

2.2 Methods

2.2.1 Extreme precipitation events in the northern Altiplano

To compute a single time series representing precipitation over the northern Altiplano, we calculated the arithmetic mean of the in-situ precipitation for each day between the 1*st* June and 31*st* August in the 1980–2010 period (Fig. 1b; PP-Andes). For each day, we averaged over all the data available in the 39 rain-gauge stations located in the northern Altiplano, resulting in a unique regional time-series of daily precipitation (Fig. 1b). We used this approach given that

the spatial distribution of rain-gauge stations in our study zone, featuring more stations in the eastern than in the western side, is maintained during the 1980–2010 period (Fig. S1b). The similar spatial distribution of rain-gauge stations across years assures that PP-Andes is not influenced by low precipitation rates from the arid western zone, even during periods with a minimum number of rain-gauge stations with available data. Next, we calculated the percentile 90 (p90; red line in Fig. 1b) of PP-Andes, and we identified days in which PP-Andes is equal or greater than p90 (0.57 mm d^{-1}). It is important to remember that 0.57 mm d^{-1} is a regional statistic, computed by using 39 stations. Furthermore, we verified that 61% of the days in our PP-Andes index equal zero, meaning that 39% of the time precipitation with values greater than zero occurs on a regional scale. We used a fixed percentile 90 (p90) instead of a seasonal value for the 1980–2010 period because the large number of days with zero precipitation in June and July decreases the value of their respective percentile 90 compared to August. Using the fixed p90 we identified 286 individual extreme precipitation events in the 1980–2010 period.

Compagnucci et al. (2001) used sequences of 5 consecutive days to properly capture the synoptic-scale circulation over South America. We applied this concept to group individual extreme precipitation events, and we proceeded as follows. For the June–August season in each year during the 1980–2010 period, we detected the first (n_1) and the second event (n_2) occurring after 1*st* June. Then, if n_1 and n_2 are separated by 5 consecutive days or less with precipitation below p90, we merged these two events into a single event (ev_1) that started in n_1 and finished in n_2. We repeated the same operation between ev_1 and a third individual event since 1*st* June (n_3). In the opposite case, n_1 is considered as a single extreme event (ev_1), and the same operation is calculated between n_2 and n_3. The final events considered for the study are indicated in Table 1. They can last between one and 16 days, with the possibility of including at most 5 consecutive days showing precipitation below the percentile 90 of PP-Andes (see Table 1). It is important to note that only eight final events show minimum precipitation equal to 0 mm day^{-1}. Following this procedure, we identified 100 winter extreme precipitation events in the northern Altiplano (100 WEPEs). We divided the WEPEs into three groups based on their duration: events lasting 1 day (42 WEPEs), 2 days (19 WEPEs) and more than 2 days (39 WEPEs).

2.2.2 Composite means and anomalies of atmospheric circulation and precipitation

In this study, we used the anomalies of horizontal wind and vertical motion, temperature, geopotential height and specific humidity, when compared to their climatology over the reference period 1980–2010. First, we computed a daily climatology for each variable from the 22*nd* May to the 10*th* September. Second, the daily climatology was temporally smoothed using a Hamming window of 5 days. Then, daily anomalies were computed by subtracting from the original data the smoothed daily climatology for each atmospheric variable. The same procedure was applied when calculating precipitation anomalies using the CHIRPS data set.

In order to describe the atmospheric processes that are associated with the onset of winter extreme precipitation events in the northern Altiplano, we used daily lead-lag composites of anomalous horizontal wind and vertical motion, specific humidity, geopotential height and temperature at different pressure levels (1000–100 hPa). The composite analysis starts four days prior - Day(-4) - to the onset of the event or Day(0). We also analyzed the regional precipitation pattern over western tropical South America using CHIRPS precipitation anomalies. The significance of the anomalies depicted in the composite analysis is evaluated using the Cramér test with a significance level of 95% (Cramér 1999), which was used in previous studies over the tropical Andes (Segura et al. 2019).

Composite analyses were also performed using the zonal-mean of atmospheric variables from 30 °S to 0 °N, and from 80 °W to 60 °W to describe the atmospheric circulation over western tropical South America. Indeed, we aim to describe the moisture transport from the western Amazon toward the northern Altiplano. In order to avoid noise, introduced by the very different atmospheric circulation to the west of the Andes, especially at lower-tropospheric levels, we proceeded as follows. For each grid-point along the latitude axis, we calculated the longitude located one degree to the west of the grid representing the highest altitude between 80 °W and 60 °W. Next, the zonal-mean was calculated by averaging the data only over the region extending from this longitude to 60 °W.

2.2.3 K-means clustering analysis

With the aim of depicting the atmospheric circulation associated with the onset of each WEPE, we applied a K-means clustering of normalized anomalies of geopotential height at 500 hPa at the initial day of each event. The normalization was done using the mean and the standard deviation of the historical daily anomalies of geopotential height at 500 hPa in each grid-point. In addition, the clustering process was separately applied to each WEPE group classified by its duration (see Sect. 2.2.1). For each WEPE group and using the silhouette method, we decided to obtain three clusters or three groups of days. The silhouette coefficient measures the relative difference between the intra-cluster distance and the distance to the next closest cluster. This means that days in each cluster have a similar spatial pattern of geopotential height at 500 hPa, that separates them from the ones in the

other two clusters. The atmospheric circulation at 850, 500, and 200 hPa associated with each cluster is computed by averaging horizontal winds, geopotential height, specific humidity, and temperature at those pressure levels in days corresponding to each cluster.

3 Winter extreme precipitation events (WEPEs) over the northern Altiplano

We identified 100 WEPEs in our zone of study (Table 1; see Sect. 2.2.1). In total, there are 286 days identified as WEPEs out of the total of 2852 days considered during the JJA season in the 1980–2010 period. The accumulated precipitation during the 100 WEPEs is 591 mm, while the total JJA precipitation for the 1980–2010 period is 728 mm. This means that WEPEs (11% of the days) are responsible for at least 81% of all JJA precipitation. Table 1 shows the precipitation characteristics of the 100 WEPEs regrouped by their duration. From all WEPEs, the maximum duration is 16 days and the maximum precipitation rate is 16.4 mm day^{-1}, occurring in the WEPE of 13 days. While WEPEs lasting 1 day are the most frequent, maximum precipitation rates are observed in WEPEs lasting more than 2 days.

Figure 1c shows the frequency of WEPEs as a function of the period of the month of their initial day or Day (0). August is the month with more occurrences of WEPEs (46) compared to June (30) and July (24). This is because WEPEs lasting more than 2 days are more frequent in August. On the other hand, WEPEs lasting 1 day have a slightly higher occurrence at the beginning of June and at the end August, while WEPEs lasting 2 days were not captured at the beginning of June, but the they are mostly equally distributed throughout the rest of the JJA season. This result indicates that the threshold of percentile 90, used in this study, could clearly identify extreme precipitation events in the JJA season, even though August shows a slight increase in the precipitation climatology. On interannual time scales (Fig. 1d), we observe two periods with high occurrence of WEPEs: the 1983–1989 period and the 2000–2004 period. Furthermore, we observe that the number of WEPEs per year is less than or equal to three since 2005. Notwithstanding the novelty of these results, which might be associated with interannual to decadal variability of the large-scale circulation (e.g. ENSO, PDO), they are beyond the scope of this study.

Atmospheric circulation at the onset of WEPEs in the northern Altiplano

The spatial patterns of mean precipitation during WEPEs lasting 1 day, 2 days, and more than 2 days are displayed in

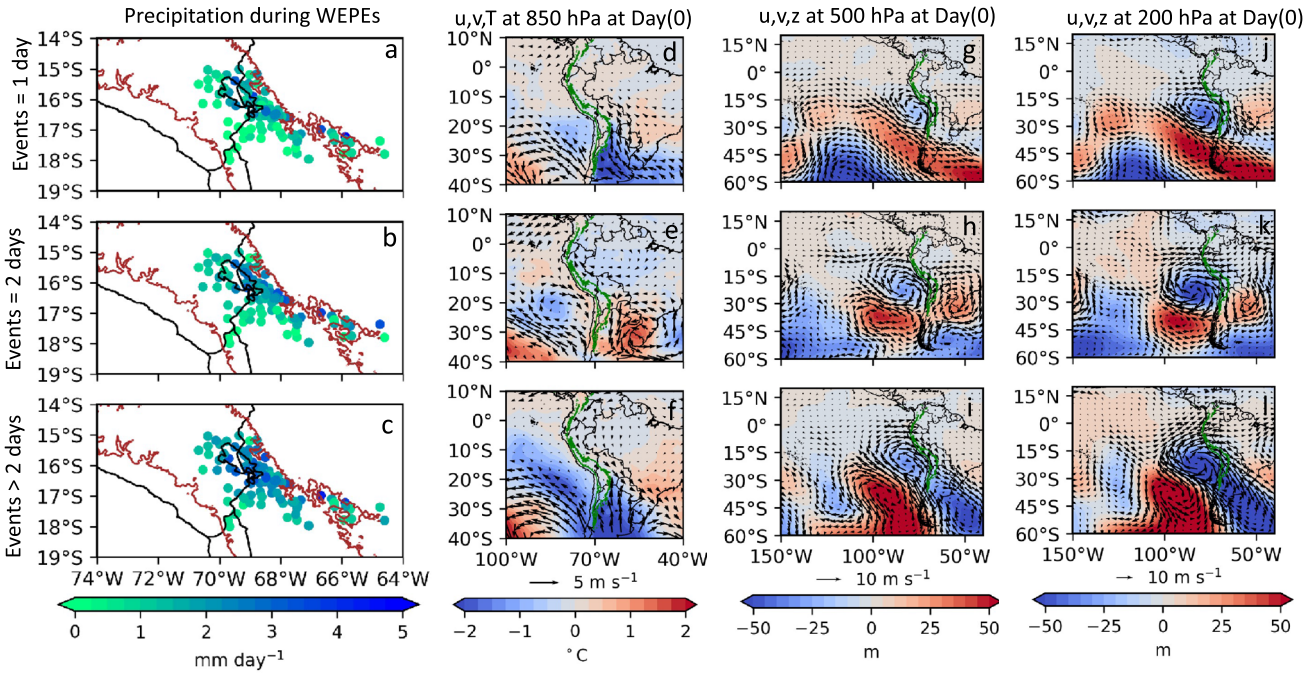

Fig. 2 **a** Mean precipitation during days of winter extreme precipitation events (WEPEs) lasting 1 day. The red line denotes the altitude of 3000 m.a.s.l. **b, c** similar to **a**, but for WEPEs lasting 2 days and more than 2 days, respectively. **d** Composite of horizontal wind (vectors) and air temperature (color shading) anomalies at 850 hPa during the initial day (D-0) of WEPEs lasting 1 day. The green line indicates the altitude of 3000 m.a.s.l. **g, j** similar to **d**, but at 500 and 200 hPa, respectively, and the color shading represents anomalies of geopotential height. **e, h, k** similar to **d, g, j** respectively, but for WEPEs lasting 2 days. **f, i, l** similar to **d, g, j**, respectively, but for WEPEs lasting more than 2 days

Fig. 2a–c, respectively. Rain-gauge stations display a progressive precipitation increase from the eastern side toward the interior of the northern Altiplano, as WEPEs lengthen in duration, meaning that WEPEs lasting more than 2 days have a larger regional impact that those lasting only 1 or 2 days.

Figure 2d–f display the associated anomalies of horizontal winds and air temperature at 850 hPa at the initial day or Day (0) of WEPEs lasting 1 day, 2 days and more than 2 days, respectively. WEPEs lasting 1 and more than 2 days are associated, at this tropospheric level, with cold temperature anomalies over extratropical South America, accompanied by southerly wind anomalies along the eastern side of the Central Andes, which are indicators of cold surges originating at higher latitudes (Fig. 2d, f, Garreaud 1999a, 2000; Vera and Vigliarolo 2000; Seluchi et al. 2006; Espinoza et al. 2013). However, the position of the leading edge of cold surges differs between groups. In addition, in WEPEs lasting more than 2 days, northerly wind anomalies over the Amazon directed toward Southeastern South America (SESA) and a strong temperature gradient along the leading edge of the cold surge are evident (Fig. 2f). Indeed, Garreaud (2000) showed that this low-level atmospheric circulation is similar to an early stage of a cold surge event, while the one associated with WEPEs lasting 1 day is similar to a late stage when the cold surge is penetrating the tropics. On the other hand, the composite of WEPEs lasting 2 days shows that low-level southerly wind anomalies have reached the equator, which explain cold anomalies over tropical South America (Fig. 2e).

At 500 hPa, anomalies of geopotential height at Day(0) of WEPEs indicate a positively tilted wave train with a northeastward orientation (moving northeastward), emanating from the Southern Pacific towards the West coast of South America (Fig. 2g–i). Negative anomalies of geopotential height accompanied by cyclonic circulation at 500 hPa are observed over the Peruvian-Chilean coast at 20 °S (Fig. 2g–i). In addition, the anomalies of geopotential height and horizontal winds at 500 hPa intensify as WEPEs exhibit longer duration. The same pattern of geopotential height and wind anomalies is observed at 200 hPa (Fig. 2j–l). Thus, the pattern of geopotential anomalies at 500 and 200 hPa over the Peruvian-Chilean coast indicate that upper-level troughs are present in the development of extreme precipitation events in the northern Altiplano.

In summary, cold surges along the eastern Central Andes as well as upper-level troughs over the Peruvian-Chilean coast are associated with heavy precipitation events over the northern Altiplano. As geopotential height anomalies at 500 hPa show an intensification as WEPEs last longer, in the next section, we classify different patterns of geopotential height anomalies at 500 hPa to identify atmospheric processes that are relevant in producing WEPEs over the northern Altiplano.

4 Classifying atmospheric circulation patterns associated with WEPEs

In this section we applied the K-means clustering analysis to anomalies of geopotential height at 500 hPa at day zero or Day(0) of WEPEs. It is well known that wave trains emanating from the southern Pacific are the main cause triggering cold surges and upper-level troughs over subtropical South America (Garreaud 2000; Vera and Vigliarolo 2000; Campetella and Possia 2006; Garreaud and Fuenzalida 2007). However, we observe in Fig. 2 that horizontal wind anomalies over the tropical West coast of South America are also important. We therefore decided to apply the clustering method to the domain 40 °S – 150 °W and 20 °N – 40 °W. We avoided analyzing anomalies of geopotential height south of 40 °S since the temporal variability in this region is strong compared with the tropical region. In addition, we performed the clustering analysis separately for WEPEs lasting 1 day, 2 days and more than 2 days. Using the silhouette method, we decided to divide each WEPE group into three clusters since the difference in the silhouette coefficient between three or four cluster is minimal (Figure S2). This means that we analyzed nine patterns of geopotential height anomalies at 500 hPa (three atmospheric clusters for each type of WEPE according to its duration). We also identified the atmospheric circulation at 200 hPa and 850 hPa, as well as the regional precipitation pattern associated with each cluster (Figs. 3, 4, 5). Using this methodology, we classified WEPES lasting 1 day in three groups. Group 1 with 15 events, Group 2 with 15 events, and Group 3 with 12 events (Fig. 3). WEPEs lasting 2 days were classified in Group 1 (8 events), Group 2 (7 events), and Group 3 (4 events) as observed in Fig. 4. WEPEs lasting more than 2 days were organized in Group 1, Group 2, and Group 3, and they are composed of 18 events, 11 events, and 10 events, respectively (Fig. 5). It is important to mention that a detailed description of each group of WEPEs can be found in the supplementary material (Text S1).

Our cluster analysis shows that at upper-levels, the anomalies of geopotential height and horizontal wind at 500 hPa and 200 hPa (Figs. 3 4, 5c, d, g, h, k, l) indicate a northeastward oriented wave train emanating from the southern Pacific. The geopotential height anomalies of this wave train have a similar pattern to the simulated in the interaction of convection over the equatorial region and the extratropical dynamics, shown by Kasahara and da Silva Dias (1986). In addition, the wave train evidenced in this study is characterized by an upper-level trough over the Peruvian-Chilean coast, which is associated with decreased atmospheric pressure and cyclonic anomalies in the mid- and upper-troposphere (Figs. 3, 4 5c, d, g, h, k,

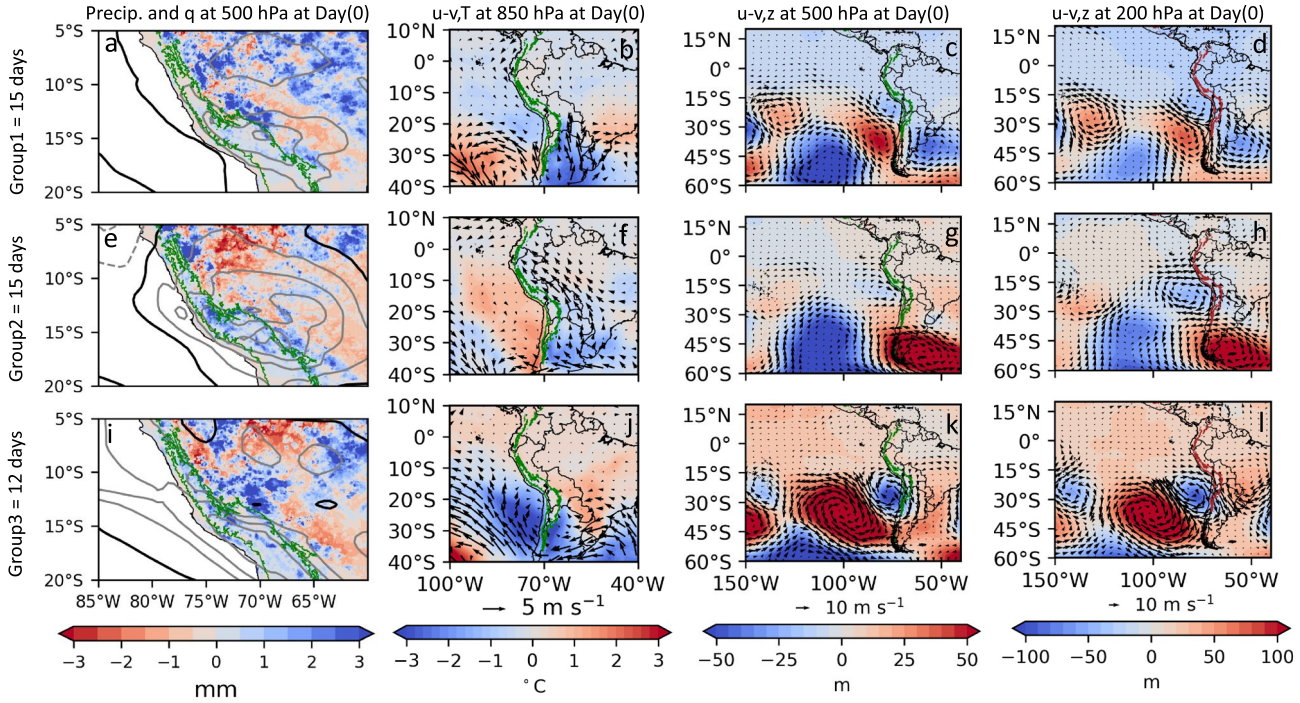

Fig. 3 **a, e, i** Composite maps of daily land precipitation anomalies, and **b, f, j** atmospheric circulation anomalies at 850, **c, g, k** at 500 and **d, h, l** at 200 hPa for the three groups based on the K-means clustering of normalized geopotential height anomalies at 500 hPa at the day 0 of winter extreme precipitation events (WEPEs) lasting 1 day. Group 1, Group 2 and Group 3 are composed of 15, 15 and 12 days, respectively. **a** Daily land precipitation (color shading) and specific humidity at 500 hPa (contours) anomalies. Positive (negative) anomalies of specific humidity are shown as solid (dashed) contours. Contour interval is 0.25 g kg^{-1}, and the contour of 0 g kg^{-1} is in black. **b** Horizontal winds (u–v; vectors) and air temperature (t; color shading) anomalies at 850 hPa. **c, d** similar to **b**, but at 500 and 200 hPa, respectively. Color shading in **c, d** represents geopotential height anomalies (z). **e, f, g, h** similar to **a, b, c, d**, respectively, but for Group 2. **i, j, k, l** similar to **a, b, c, d**, respectively, but for Group 3. The 3000 m.a.s.l. contour is shown as a green line

l). An important property of upper-level troughs is their capacity to trigger heavy precipitation events when they encounter regions where the lower- and mid-troposphere exhibit a high moisture content (Hoskins et al. 1985; Cox et al. 1995; Kiladis 1998; Knippertz 2007). Indeed, all clusters show an anomalous air moistening at 500 hPa at Day0 of the event (Figs. 3 4 5c, d, g, h, k, l).

Despite the similarities in anomalies of specific humidity at 500 hPa, the cluster analysis reveals differences in the spatial pattern of precipitation between the western Amazon and the Altiplano. 27 WEPEs lasting 1 day (Group 1 and Group2), four WEPEs lasting 2 days (Group 3) and 28 WEPEs lasting more than 2 days (Group 1 and Group 3) show wet condition over the western Amazon and the Altiplano. Positive precipitation anomalies in both regions, observed in these 51 WEPEs, are explained by the position of low-level southerly wind anomalies over subtropical South America (Figs. 3b, j; 4j; 5b, j). Indeed, southerly wind anomalies at 850 hPa, accompanied by negative temperature anomalies south of 20 °S, indicate the presence of a cold surge along the eastern Central Andes, which has been signaled as an important factor for triggering deep convection and precipitation over the southern and western Amazon (Wang and Fu 2004; Espinoza et al. 2013; Sicart et al. 2016; Paccini et al. 2018). Furthermore, low-level northerly wind anomalies over the western Amazon and the SESA region in Group 1 of WEPEs lasting more than 2 days indicate an intensified southward moisture transport, characteristic of an anomalous South American Low-Level Jet (Fig. 5b). Warm air temperature anomalies over the SESA region denote a strong temperature and pressure gradient, which is associated with a cold surge propagating into tropical regions in the following days (Garreaud 1999a, 2000; Vera and Vigliarolo 2000). It is important to note that, unlike the other groups, Group 3 of WEPEs lasting more than 2 days is most frequent in August (Figure S3). Indeed, WEPEs lasting 1 and 2 days are more equally distributed in June, July, and August (Figure S3).

On the other hand, 41 WEPEs composed of 15 WEPEs lasting 1 day (Group 1), 15 lasting 2 days (Group 1 and Group 2), and 11 WEPEs lasting more than 2 days show a strong precipitation dipole between the western Amazon (dry) and the Altiplano (wet; Figs. 3e; 4a, e; 5e). This precipitation dipole can be explained by the circulation at 850

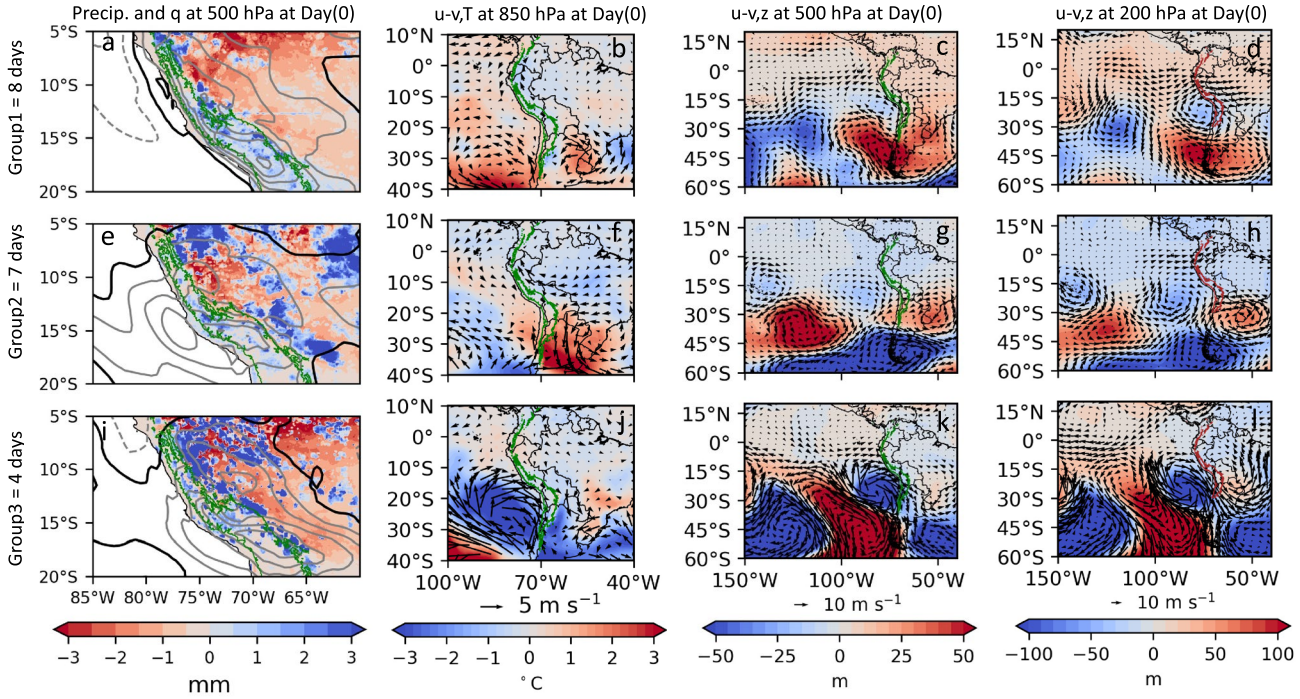

Fig. 4 Similar to Fig. 3, but for WEPEs lasting 2 days. Group 1, Group 2 and Group 3 are composed of 8, 7 and 4 days, respectively

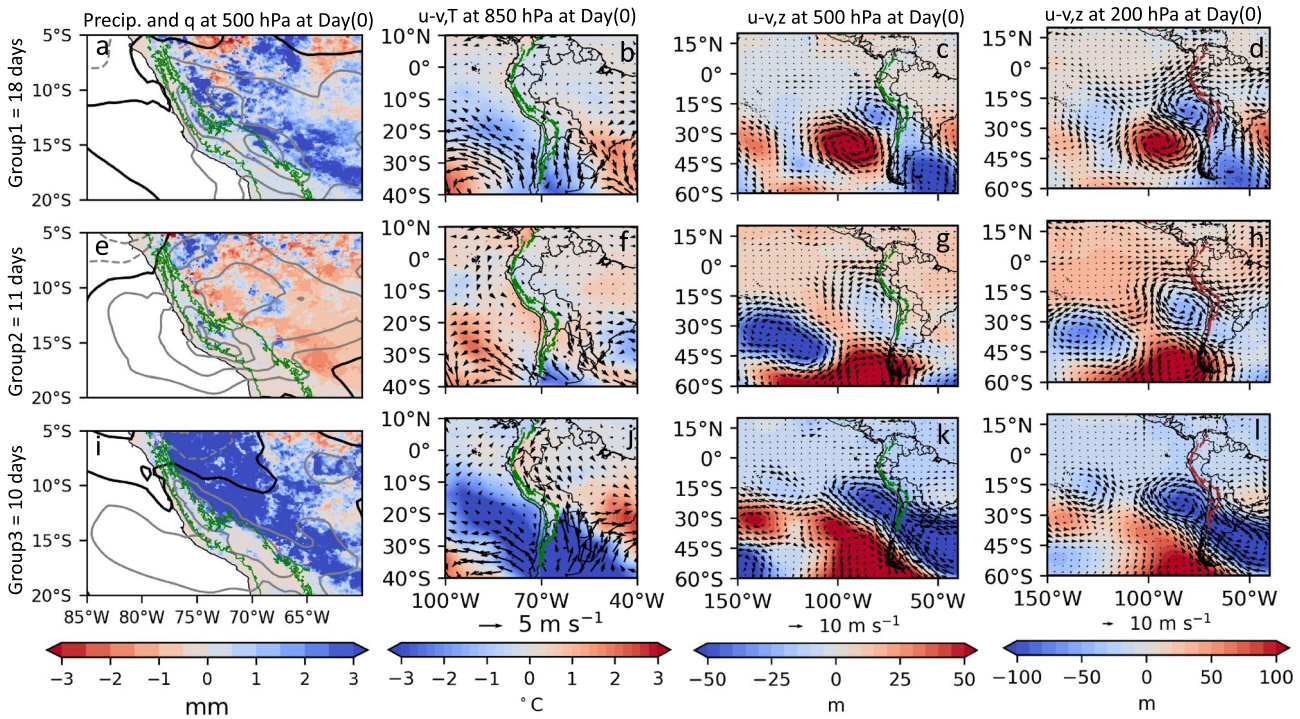

Fig. 5 Similar to Fig. 3, but for WEPEs lasting more than 2 days. Group 1, Group 2 and Group 3 are composed of 18, 11 and 10 days, respectively

Table 1 Characteristics of winter extreme precipitation events in the northern Altiplano

Lifetime (days)	Total number of events	Total PP (mm)	Max PP (mm)	Min PP (mm)	Mean PP (mm)
1	42	45.2	3.2	0.6	1.1
2	19	53.6	4.2	0.6	1.4
3	8	51.6	6.3	0.6	2.2
4	4	23.6	3.8	0.5	1.5
5	8	105.8	13.7	0.0	2.6
6	2	17.2	3.5	0.2	1.4
7	7	66.3	7.6	0.0	1.4
8	2	28.2	6.2	0.0	1.8
9	1	24.7	7.9	0.3	2.7
10	2	27.5	4.9	0.0	1.4
11	1	13.6	3.2	0.0	1.2
12	2	77.4	13.6	0.0	3.2
13	1	36.7	16.4	0,1	2.8
16	1	20.0	4.3	0.0	1.2
Total	100	591.0			

The first column shows the lifetime of WEPEs in days, while the second column indicates the number of total WEPEs for each lifetime category. The total, maximum, minimum, and mean precipitation during WEPEs of different duration are displayed in column three, four, five and six, respectively

hPa, which in these groups is characterized by southerly wind anomalies at the equator and along the eastern equatorial Andes (Figs. 3f; 4b, f; 5f). Concordantly, several studies have shown that, while the leading edge of this low-level southerly regime enhances convection, the back edge is associated with subsidence and dry conditions (Garreaud 1999a, 2000; Wang and Fu 2004; Espinoza et al. 2013; Sicart et al. 2016; Paccini et al. 2018).

Thus, there is likely an association between the upper-level trough over the Peruvian-Chilean coast and the different stages of southerly anomalies originating from subtropical South America. One set of WEPEs (41 WEPEs) is related to an upper-level trough over the Peruvian-Chilean coast and low-level southerly wind anomalies crossing the equator, while the other groups (59 WEPEs), also associated with the upper-level trough, are characterized by low-level southerly wind anomalies along the Central Andes (20°S). While these mechanisms can explain the dynamics of WEPEs, there are remain questions regarding the mechanisms described above and how moisture transport from the western Amazon toward the Altiplano occurs. These aspects are discussed in the next sections.

5 Three mechanisms triggering WEPEs in the northern Altiplano

As explained in the previous section, the 100 WEPEs are strictly associated with an upper-level trough over the Peruvian-Chilean coast and increases in mid-tropospheric moisture over the western Amazon and the Altiplano. However, the differences in circulation at 850 hPa between two groups of WEPEs suggest different mechanisms of atmospheric moisture transport from the western Amazon to the Altiplano. In this section, we focus our attention on the atmospheric circulation during the onset of 59 WEPEs associated with cold surges along the eastern slopes of the Central Andes. Since these 59 WEPEs show similar circulation anomalies, we decided to merge them into a single group, meaning that Group 1 and 3 of WEPEs lasting 1 day, Group 3 of WEPEs lasting 2 days, and Groups 1 and 3 of WEPEs lasting more than three days were combined in a single composite. As the composite analysis was computed using 59 WEPEs, we were able to calculate the significance of the anomalies at the 95% significance level.

From Day(-4) to Day(-2), significant and positive precipitation anomalies over equatorial South America intensify in the western region and show slight southward propagation towards the western Amazon (Fig. 6a–c). At 850 hPa, the southward propagation of convective activity toward the western Amazon is consistent with the strengthening of northerly wind anomalies that reach subtropical regions at Day(-2). On Day(-1) and Day(0), we observe that the northward propagation of precipitation has stalled over the western Amazon (Fig. 6d, e). Similar behavior is noticed in northerly wind anomalies at 850 hPa, which are not extending southward of 20 °S over South America (Fig. 6i, j). On the other hand, significant positive precipitation anomalies over the northern Altiplano are accompanied by the arrival of a cold surge along the eastern Central Andes (Fig. 6e, j).

The lead-lag daily composite analysis of the anomalous zonal-mean of meridional wind and vertical motion,

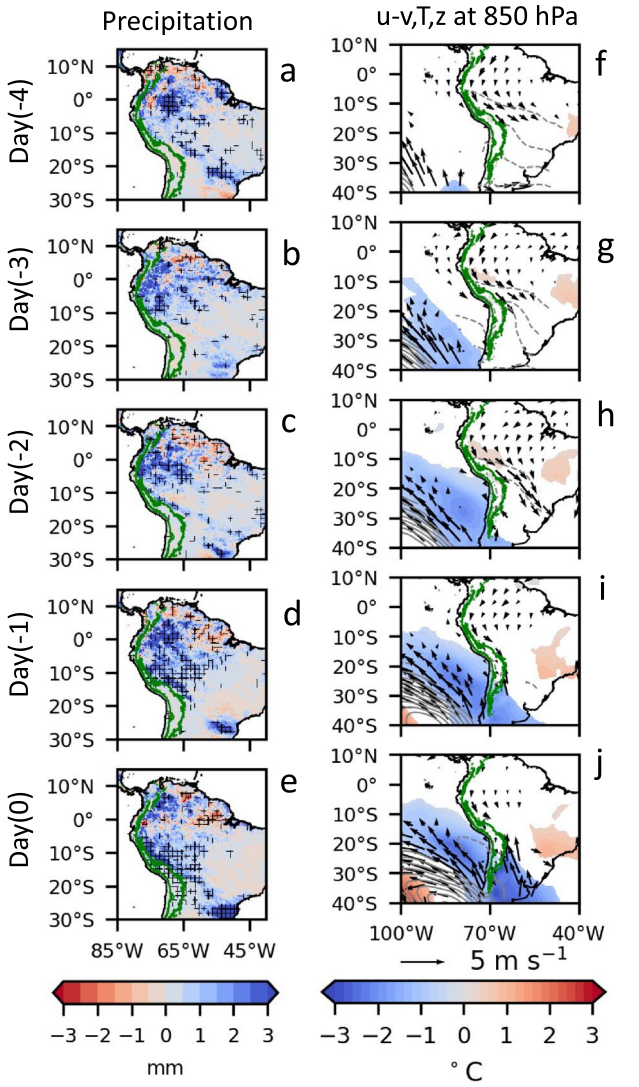

Fig. 6 Daily lead-lag composite maps based on winter extreme precipitation events (WEPEs) over the northern Altiplano associated with low-level northerly wind anomalies over the western Amazon, a cold surge along the eastern Central Andes, and an upper-level trough over the Peruvian-Chilean coast (59 WEPEs). The composite analysis is from four days before—Day(-4)—to the initial day—Day(0)—of the WEPEs. **a**–**e** Anomalies of precipitation, and significant precipitation anomalies are marked with a black cross. **f**–**j** Anomalies of horizontal winds (u–v; vector), air temperature (T; color shading) and geopotential height (z; contour) at 850 hPa. Positive (negative) anomalies of geopotential height are shown in solid (dashed) contours. The contour interval of geopotential height is 10 m. Only anomalies with a significance at 95%, using the Cramer test, are displayed (p-values < 0.05). In the case of horizontal winds, vectors are only shown when anomalies in either u or v are significant at 95% using the Cramer test. In **a**–**j** the 3000 m.a.s.l. contour is shown as a green line

as well as zonal wind and specific humidity anomalies over western tropical South America (80 °W – 60 °W, see Sect. 2.2.2), are shown in Fig. 7a–e. Low-level northerly wind anomalies over the western Amazon (north of 20 °S) strengthen from Day(-4) to Day(-2), and they are accompanied by significant lower-tropospheric moistening in the same region (Fig. 7a–c). We need to remark that the lack of strong anomalies of upward motion over equatorial South America could be explained by the fact that convection is localized, as observed in the strong anomalies of precipitation in Fig. 6a, b. On Day(-2), weak significant anomalies of upward motion are observed at the leading edge of the low-level northerly anomalies, but strong anomalous upward motion above 500 hPa is observed over the tropical Andes south of 15 °S (Fig. 7c). Indeed, significant upper-level westerly wind anomalies south of 20 °S indicate the arrival of the eastern side of the upper-level trough over the Andes (see contour lines in Fig. 7c).

On Day(-1), the mid-troposphere over the western Amazon significantly moistens, explained by the intensification of upward motion over the western Amazon (Fig. 7d). The mid-tropospheric moistening and the anomalous upward motion over the western Amazon, observed in Fig. 7d, are consistent with the development of precipitation in this Amazon region shown in Fig. 6d. South of 20 °S, the composite analysis show significant anomalies of vertical motion as a result of the interaction of the leading edge of the cold surge with the eastern side of the upper-level trough over the Andes (Fig. 7d). On Day(0), humidity and vertical motion anomalies have intensified over the Altiplano, explaining the significant increase of precipitation.

It is known that cold surges produce upward motion along their leading edge, reaching mid-tropospheric levels during the JJA season (Garreaud 1999a, 2000; Espinoza et al. 2013; Bowerman et al. 2017). However, Fig. 7d,e shows that the ascending branch at the leading edge of the cold surge reaches the upper-troposphere over the Altiplano, specifically in the same zone where the eastern side of the upper-level trough is centered. Furthermore, they jointly propagate northward. Thus, the interaction between the upper-level trough and the cold surge also plays a major role in promoting ascending motion over the Altiplano. We suggest that this association is also related to the advection of cold air from the cold surge to the upper-level trough. This is an important feature since convection warms the core of the upper-level trough, decreasing its cyclonic vorticity and terminating the system (Hoskins et al. 1985; Garreaud and Fuenzalida 2007). Thus, cold air advection by the cold surge could keep the upper-level trough alive, explaining the reason for some long-lasting events, even if latent heat due to convection is released at mid- and upper-tropospheric levels over the Altiplano. This is an important topic that deserves a more in-depth analysis in future studies.

As stated above, upper-level westerly wind anomalies over the Altiplano indicate the presence of an upper-level trough emanating from the eastern Pacific. Thus, we

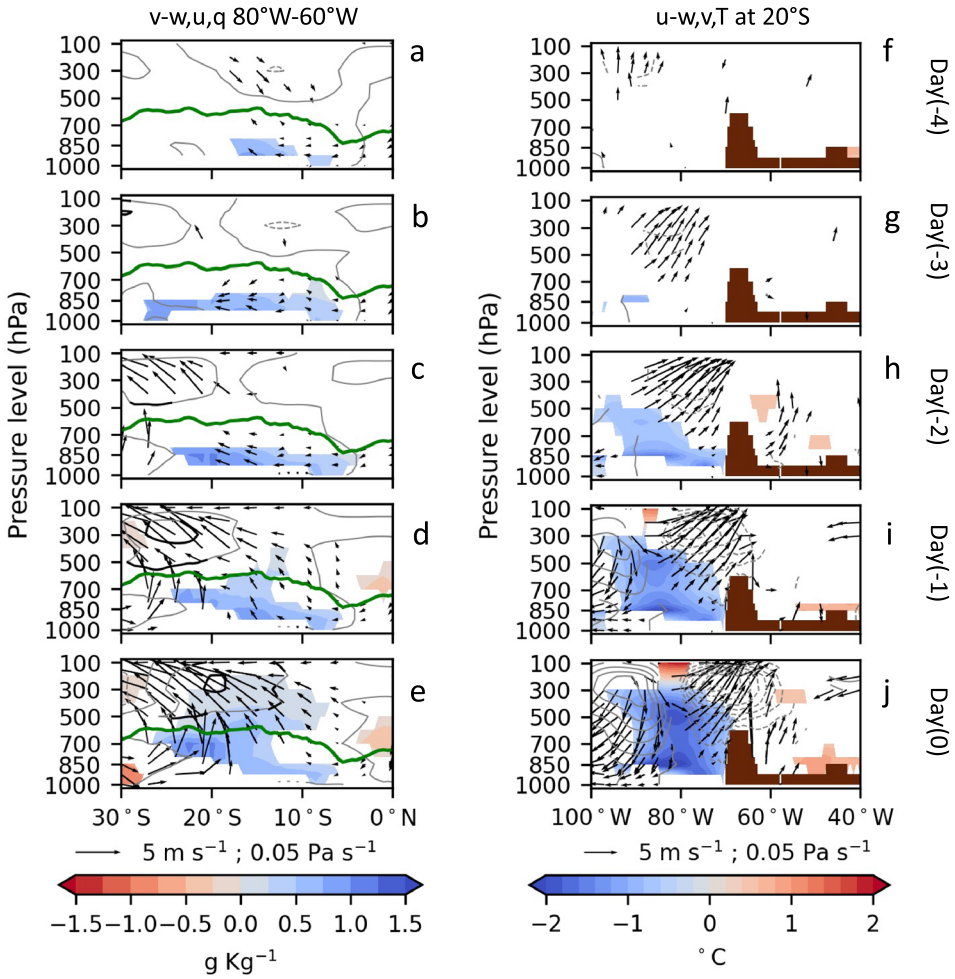

Fig. 7 Daily lead-lag composite maps based on winter extreme precipitation events (WEPEs) over the northern Altiplano associated with low-level northerly wind anomalies over the western Amazon, a cold surge along the eastern Central Andes, and an upper-level trough over the Peruvian-Chilean coast (59 WEPEs). The composite analysis is from four days before—Day(-4)—to the initial day—Day(0)—of the WEPEs. **a–e** Zonal-mean of meridional wind-vertical motion (v–w; vectors), zonal wind (u; contours) and specific humidity (color shading) anomalies over western tropical South America (80 °W – 60 °W;30 °S – 0 °N; see Sect. 2.2.2). Contour interval of u is 2 m s^{-1}. The green line denotes the highest altitude between 80 °W – 60 °W. **f–j** Pressure-longitude cross-section at 20 °S for anomalies of zonal wind-vertical motion (u–w; vectors), meridional winds (v; contours) and air temperature (T; color shading). Solid (dashed) contours indicate positive (negative) anomalies of v. The contour interval of v is 2 m s^{-1}. The Andes profile at 20 °S is shown in brown. In **a–j**, only anomalies with a significance at 95%, using the Cramer test, are displayed (p-values < 0.05). For zonal winds in **a–e**, significant anomalies are shown as black solid contours. In the case of v–w (u–w) in **a–e** (**f–j**), vectors are only shown when anomalies in either v or w (u or w) are significant at 95% using the Cramer test

computed a lead-lag composite analysis of the vertical structure of anomalous air temperature, zonal and meridional wind and vertical motion at 20 °S between 100 °W and 40°W (Fig. 7f–j). As several studies have stated, upper-level troughs are characterized by ascending motion over their eastern region and subsidence on their western side (Hoskins et al. 1985; Cox et al. 1995; Kiladis 1998; Knippertz 2007). In addition, cold air temperature anomalies at mid- and upper-tropospheric levels and warm anomalies above 200 hPa, the latter associated with tropopause folding, are distinctive characteristics of upper-level troughs. These features are observed in Fig. 7f–j, in which significant upper-level northerly (southerly) wind anomalies along the eastern (western) side of the upper-level trough are accompanied by significant anomalous upward motion (subsidence) along the eastward propagation of the upper-level trough. Cold (warm) air temperature anomalies below (above) 200 hPa are also noticed at the core of the upper-level trough (Fig. 7h–j). We observe an intensification of wind and temperature anomalies while the upper-level trough approaches the Altiplano (Fig. 7f–j). On Day(0), anomalous upward motion over the Altiplano and over the western Amazon is, indeed,

associated with the placement of the eastern branch of the upper-level trough over these two regions (Fig. 7j).

Even if the upper-level trough over the Peruvian-Chilean coast and the cold surge east of the central Andes are the principal components of the upward motion over the Altiplano, significant lower- and mid-tropospheric moistening over the western Amazon before the onset of these 59 WEPEs also plays an important role in the Altiplano precipitation. This means that these 59 WEPEs can be explained by the associated of these three mechanisms (i) lower- and mid-tropospheric moistening over the western Amazon before the onset of WEPEs, (ii) a cold surge arriving east of the eastern Central Andes, and (iii) an upper-level trough over the Peruvian-Chilean coast. It is important to mention that snowfall events associated with cut-off lows as described by Vuille and Ammann (1997) also form part of the WEPEs associated with these three atmospheric components.

6 Two mechanisms triggering precipitation over the northern Altiplano

In Sect. 4, 41 WEPEs were characterized as being associated with an upper-level trough over the Altiplano and low-level southerlies crossing the equator on Day(0) of the event, meaning that the mechanisms to transport moisture from the western Amazon to the Altiplano are different than those observed in Sect. 5. To address this question, we used a composite analysis of anomalous atmospheric circulation at different pressure levels and precipitation from four days before the initial day of the event (Fig. 8). We combined in a single composite Group 2 of WEPEs lasting 1 day, Group 1 and 2 of WEPEs lasting 2 days, and Group 2 of WEPEs lasting more than 2 days.

From 4–2 days prior to the development of heavy precipitation over the northern Altiplano, the western Amazon presents increased precipitation (Fig. 8a–c). These precipitation anomalies are explained by the southerly wind incursion from subtropical South America to the equatorial region, as observed in the zonal-mean of meridional wind and vertical motion anomalies, which shows the equatorward progression of low-level meridional wind anomalies (Fig. 8f–h). Furthermore, the southerly wind incursion triggers upward motion acceleration along its leading edge, and as a consequence, low-level moisture is transported to mid-tropospheric levels (Fig. 8f–h). The intense low-level southerly wind incursion is explained by the subsidence south of 20 °S, which is responsible for the northward advection of anticyclonic vorticity from the extratropics, adding momentum for the incursion to reach equatorial regions (Fig. 8f-h; Garreaud 1999a, 2000; Vera and Vigliarolo 2000; Espinoza et al. 2013).

On Day(-1), the southerly incursion continues its northward propagation, but anomalous upward motion is observed above 500 hPa south of 10 °S. This upward acceleration cannot be explained by the low-level southerly wind incursion since upward motion generated by this mechanism tends to be restricted to the lower- and mid-troposphere. Indeed, the acceleration of upward motion in the upper-troposphere results from the arrival of the upper-level trough. Furthermore, moisture anomalies in the mid-troposphere between 15 °W and 10 °S increased. We hypothesize that the combination of the upper-level trough and the leading edge of the southerly wind incursion, indeed, enhanced this upward moisture transport. On Day(0), the significant increase of precipitation in the Altiplano region is explained by the moistening of the mid-troposphere over the Altiplano and the upward motion acceleration due to the presence of the upper-level trough (Fig. 8j). On the other hand, the decrease of precipitation over the western Amazon is a characteristic of low-level southerly winds crossing the equator, associated with low-level subsidence, as observed in Fig. 8j.

Thus, the 41 WEPEs analyzed in this section, even if they are associated with an upper-level trough, are characterized by a different role of the low-level southerly wind anomaly as compared to the 59 WEPEs described in Sect. 5. Indeed, the composite analysis shows that the incursion of low-level southerly anomalies into equatorial South America, enhances upward moisture transport over the western Amazon that the upper-level trough uses to trigger precipitation over the Altiplano.

7 Conclusion

Extreme winter precipitation events over the northern Altiplano (18 °S – 15 °S; > 3000 m.a.s.l.) are one of the extreme weather conditions that causes considerable damage to social and economic activities in this Andean region. In this study, we made use of 39 rain-gauge stations located over the northern Altiplano and we identified 100 winter extreme precipitation events (WEPEs) for June–August seasons in the 1980–2010 period. The duration of these events varies between 1 and 16 days. In general, long-lasting WEPEs (more than 2 days; 39 WEPEs) are characterized by spatially more wide-spread precipitation, extending over much of the northern Altiplano, while precipitation during WEPEs lasting one (42 WEPEs) and 2 days (19 WEPEs) is spatially constrained to the eastern side of the northern Altiplano.

The K-means clustering method was applied separately to geopotential height anomalies at 500 hPa at the initial day or Day(0) of WEPEs lasting 1 day, 2 days, and more than 2 days, respectively. This analysis showed that WEPEs are principally associated with two characteristic circulation types over tropical South America in the austral winter: (i) a low-level southerly wind incursion into tropical regions, and (ii) an upper-level trough over the Peruvian-Chilean coast.

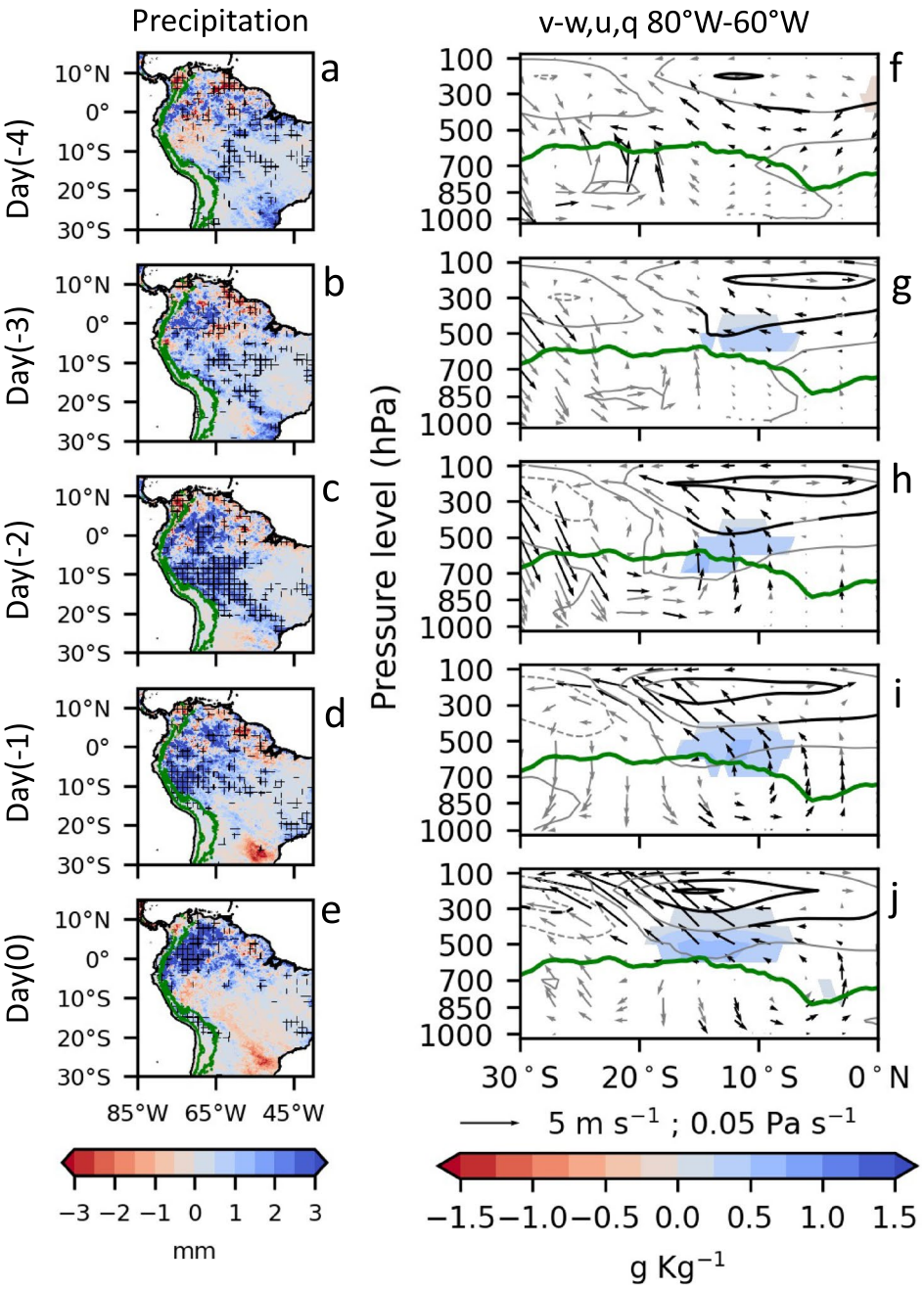

Fig. 8 Daily lead-lag composite maps based on winter extreme precipitation events (WEPEs) over the northern Altiplano lasting 1 day and associated with low-level southerly winds crossing the equator and an upper-level trough over the Peruvian-Chilean coast (41 WEPEs). The composite analysis is from four days before—Day(-4)—to the initial day—Day(0)—of the WEPEs. **a**–**e** Anomalies of precipitation. Significant precipitation anomalies are marked with a black cross. **f**–**j** Zonal-mean of meridional wind-vertical motion (v–w; vectors), zonal wind (u; contours) and specific humidity (color shading) anomalies over western tropical South America (80 °W – 60 °W;30 °S – 0 °N; see Sect. 2.2.2). Contour interval of u is 2 m s^{-1}. The green line denotes the highest altitude between 80 °W and 60 °W. In **a**–**j**, only anomalies with a significance at 95%, using the Cramer test, are displayed (p-values < 0.05). For zonal winds in **f**–**j**, significant anomalies are shown as black solid contours. In the case of v–w in **f**–**j**, vectors are only shown when anomalies in either v or w are significant at 95% using the Cramer test

However, the cluster analysis also shows that 59 WEPEs, composed of 27 WEPEs lasting 1 day, four WEPEs lasting 2 days, and 28 WEPEs lasting more than 2 days, are characterized on Day(0) by low-level southerly wind anomalies along the Central Andes. The other 41 WEPEs, composed of 15 WEPEs lasting 1 day, 15 WEPEs lasting 2 days, and 11 WEPEs lasting more than 2 days, are explained by low-level southerly wind anomalies over equatorial regions.

The difference in circulation at 850 hPa between these two groups means that the interaction between the upper-level trough and the low-level southerly wind anomalies differs. Indeed, the lead-lag composite analysis on the 59 WEPEs revealed the following characteristics. Before the onset of WEPEs, a lower-tropospheric moistening, associated with low-level northerly wind anomalies, is observed over the western Amazon, indicating an important role of the tropical circulation. On Day(-1), a cold surge arrives to the east of the northern Central Andes (20 °S), inducing convection and precipitation over this Andean region. In addition, the eastern side of the upper-level trough reaches the Altiplano on Day(-1), intensifying convection over the Central Andes. On Day(0), the core of the upper-level trough and the

leading edge of the low-level southerly wind anomaly align at the latitude of the Altiplano. Furthermore, the coupling of these two mechanisms intensifies the moisture transport from the western Amazon to the Altiplano on Day(0). Thus, three mechanisms are explaining these 59 WEPEs: (i) the low-level northerly wind anomalies over the western Amazon prior to the onset of WEPEs, (ii) the low-level southerly wind anomalies along the central Andes, and (iii) the upper-level trough over the Peruvian-Chilean coast.

The daily lead-lag composite analysis of the 41 WEPEs associated with the low-level southerly wind regime crossing the equator and the upper-level trough over the Peruvian-Chilean coast describes another mechanism of transporting moisture from the western Amazon toward the Altiplano. Low-level southerly winds that crossed the equator lift moist air from lower- to mid-tropospheric levels over the western Amazon on Day(-2). From Day(-1) to Day(0), the upper-level trough helps transporting moisture toward the Altiplano, where precipitation initiates on Day(0). Furthermore, we can observe that these types of WEPEs are also characterized by a precipitation dipole between the western Amazon and the Altiplano. Hence, in these WEPEs, we only observe the interaction of two mechanisms: (i) the low-level southerly wind anomalies crossing the equator and (ii) the upper-level trough over the Peruvian-Chilean coast.

Thus, the 39 rain-gauge stations used in this study allowed identifying the extreme winter precipitation events over the northern Altiplano and their associated mechanisms. Nevertheless, it is important to keep in mind that most of these rain-gauge stations are located on the eastern side of the northern Altiplano. Thus, a question to address in the future, is to assess the influence of the atmospheric mechanisms presented in this study for extreme precipitation events over the western part of our study region. Furthermore, the interaction of these regional atmospheric circulation systems with the diurnal cycle of precipitation over the Altiplano should be investigated as done in the Amazon basin (Nunes et al. 2016). This point is important to mention, especially regarding WEPEs characterized by anomalous low-level northerly winds over the western Amazon prior to extreme events. As those winds carry moisture to the Andes-Amazon transition, the upslope wind circulation due to the difference in heating between the lowlands and the mountain could enhance moisture transport toward the Altiplano. Indeed, Junquas et al. (2018) showed that the diurnal cycle of precipitation over the Altiplano responds to the diurnal cycle of winds, especially due to the moisture transport from the Amazon to the highlands.

One point to highlight is that convection over the western Amazon, especially at the equator prior to the arrival of WEPEs, could facilitate the northward propagation of cold surges, due to the influence of tropical convection on the general circulation (Gill 1980). Convection over equatorial South America facilitates the development of an upper-level anticyclone south of the heat source (Rossby wave response), and this could reinforce the upper-level high pressure system entering subtropical South America, responsible for the cold surge. Simultaneously, once the cold surge starts to trigger convection over tropical South America, convection over equatorial South America weakens, thereby decreasing subsidence over the Altiplano and allowing convection to enhance. Since the heat source over tropical South America deserves major attention regarding its contribution to WEPEs, future studies should focus on this tropical mechanism to better quantify its role.

On a regional scale, the upper-level trough and low-level southerly anomalies associated with WEPEs perturb the tropospheric circulation over western tropical South America in a way that could potentially also induce heavy precipitation events over other regions of the upper-elevation tropical Andes (> 3000; 20 °S – 0 °N). As convection over equatorial South America may be an important factor to enhance precipitation over the Altiplano, tropical intraseasonal variability impacting South American weather, such as the MJO (Mayta et al. 2019) could influence the synoptic conditions prevailing during WEPEs. Another topic that we did not explore in this study, but which is of potential relevance for studies on interannual and interdecadal timescales, is the influence of large-scale coupled modes of ocean–atmosphere variability, such as the ENSO and the Pacific Decadal Oscillation on the occurrence of WEPEs.

Supplementary Information The online version contains supplementary material available at https://doi.org/10.1007/s00382-022-06240-1.

Acknowledgements Research funding comes from the AMANECER-MOPGA project funded by ANR and IRD (ref. ANR-18-MPGA-0008) and the IDEX grants of the University Grenoble Alpes (UGA), the VASPAT project IDEX "IRS-Initiative de Recherche Stratégique" (part of the ANR project ANR-15-IDEX-02) of UGA. The IGE's authors thanks the support of the Labex OSUG@2020 (Investissements d'avenir - ANR10 LABX56). Furthermore, Mathias Vuille was partially supported by NSF awards AGS-1702439, OISE-1743738, and EAR-2103041. The quality of this research was improved by the constant exchange of ideas with members of the C2H team from the IGE. We give special thanks to J. Ronchail, L. Li, Pedro Silva-Dias, Myriam Khodri, Serge Janicot and Vincent Moron for their contributions in the framework of H. Segura's PhD. thesis committee.

Author contributions All authors contributed to the study's conception and design. Material preparation, data collection, and analysis were performed by HS and JCE. The first draft of the manuscript was written by HS. JCE, CJ, TL, MV, and TC commented and edited on previous versions of the manuscript. All authors read and approved the final manuscript.

Funding No funding was received for conducting this study.

Data availability The in-situ precipitation data set analyzed during the current study are from the Data on climate and Extreme weather for the Central Andes (DECADE) project, and it could be downloaded from

this link: https://www.geography.unibe.ch/research/climatology_group/research_projects/decade/index_eng.html.

Code availability The custom codes used to analyze the data sets in the current study are available from the corresponding author on reasonable request.

Declarations

Conflict of interest The authors have no conflicts of interest to declare that are relevant to the content of this article.

Ethical approval Not applicable.

Consent to participate Not applicable.

Consent for publication Not applicable.

References

Alvarez MS, Vera CS, Kiladis GN, Liebmann B (2013) Intraseasonal variability in South America during the cold season. Clim Dyn. https://doi.org/10.1007/s00382-013-1872-z

Andrade MFE (2018) Clima y eventos extremos del Altiplano Central perú-boliviano/climate and extreme events from the Central Altiplano of Peru and Bolivia 1981–2010. Geographica Bernensia. https://doi.org/10.4480/GB2018.N01

Bendix J, Lauer W (1992) Die Niederschlagsjahreszeiten in Ecuador und ihre klimadynamische Interpretation (Rainy Seasons in Ecuador and Their Climate-Dynamic Interpretation). Erdkunde 2(1992):118–134. http://www.jstor.org/stable/25646379

Boers N, Barbosa HMJ, Bookhagen B, Marengo JA, Marwan N, Kurths J (2015) Propagation of strong rainfall events from southeastern South America to the central andes. J Clim 28(19):7641–7658. https://doi.org/10.1175/JCLI-D-15-0137.1

Bonshoms M, Álvarez-Garcia FJ, Ubeda J, Cabos W, Quispe K, Liguori G (2020) Dry season circulation-type classification applied to precipitation and temperature in the Peruvian Andes. Int J Climatol. https://doi.org/10.1002/joc.6593

Bowerman AR, Fu R, Yin L, Fernando DN, Arias PA, Dickinson RE (2017) An influence of extreme southern hemisphere cold surges on the North Atlantic Subtropical High through a shallow atmospheric circulation. J Geophys Res Atmos 122(19):10135–10148. https://doi.org/10.1002/2017JD026697

Campetella CM, Possia NE (2006) Upper-level cut-off lows in southern South America. Meteorol Atmos Phys 96(1–2):181–191. https://doi.org/10.1007/s00703-006-0227-2

Chavez SP, Takahashi K (2017) Orographic rainfall hot spots in the Andes-Amazon transition according to the TRMM precipitation radar and in situ data. J Geophys Res Atmos 122(11):5870–5882. https://doi.org/10.1002/2016JD026282

Compagnucci RH, Araneo D, Canziani PO (2001) Principal sequence pattern analysis: a new approach to classifying the evolution of atmospheric systems. Int J Climatol 21(2):197–217. https://doi.org/10.1002/joc.601

Cox BD, Bithell M, Gray LJ (1995) A general circulation model study of a tropopause-folding event at middle latitudes. Q J R Meteorol Soc 121(524):883–910. https://doi.org/10.1002/qj.49712152408

Cramér H (1999) Mathematical methods of statistics. Princeton mathematical series, Princeton University Press. https://books.google.fr/books?id=CRTKKaJO0DYC

Dee DP, Uppala SM, Simmons AJ, Berrisford P, Poli P, Kobayashi S, Andrae U, Balmaseda MA, Balsamo G, Bauer P, Bechtold P, Beljaars AC, van de Berg L, Bidlot J, Bormann N, Delsol C, Dragani R, Fuentes M, Geer AJ, Haimberger L, Healy SB, Hersbach H, Hólm EV, Isaksen L, Kållberg P, Köhler M, Matricardi M, Mcnally AP, Monge-Sanz BM, Morcrette JJ, Park BK, Peubey C, de Rosnay P, Tavolato C, Thépaut JN, Vitart F (2011) The ERA-Interim reanalysis: configuration and performance of the data assimilation system. Q J R Meteorol Soc 137(656):553–597. https://doi.org/10.1002/qj.828

Eghdami M, Barros AP (2019) Extreme orographic rainfall in the eastern Andes tied to cold air intrusions. Front Environ Sci 7(JUL):1–18. https://doi.org/10.3389/fenvs.2019.00101

Espinoza JC, Ronchail J, Frappart F, Lavado W, Santini W, Guyot JL (2013) The major floods in the Amazonas River and Tributaries (Western Amazon Basin) during the 1970–2012 Period: a focus on the 2012 flood*. J Hydrometeorol 14(3):1000–1008. https://doi.org/10.1175/JHM-D-12-0100.1

Espinoza JC, Chavez S, Ronchail J, Junquas C, Takahashi K, Lavado W (2015) Rainfall hotspots over the southern tropical Andes: spatial distribution, rainfall intensity, and relations with large-scale atmospheric circulation. Water Resour Res 51(5):3459–3475. https://doi.org/10.1002/2014WR016273

Espinoza JC, Garreaud R, Poveda G, Arias PA, Molina-Carpio J, Masiokas M, Viale M, Scaff L (2020) Hydroclimate of the Andes part I: main climatic features. Front Earth Sci 8(March):1–20. https://doi.org/10.3389/feart.2020.00064

Espinoza JC, Arias PA, Moron V, Junquas C, Segura H, Sierra-Pérez JP, Wongchuig S, Condom T (2021) Recent changes in the atmospheric circulation patterns during the dry-to-wet transition season in South Tropical South America (1979–2020): impacts on precipitation and fire season. J Clim 34(22):9025–9042. https://doi.org/10.1175/JCLI-D-21-0303.1

Figueroa SN, Satyamurty P, Da Silva Dias PL (1995) Simulations of the summer circulation over the South American Region with an Eta Coordinate Model. J Atmos Sci 52(10):1573–1584. https://doi.org/10.1175/1520-0469(1995)052<1573:SOTSCO>2.0.CO;2

Figueroa M, Armijos E, Espinoza JC, Ronchail J, Fraizy P (2020) On the relationship between reversal of the river stage (repiquetes), rainfall and low-level wind regimes over the western Amazon basin. J Hydrol Reg Stud. https://doi.org/10.1016/j.ejrh.2020.100752

Funk C, Peterson P, Landsfeld M, Pedreros D, Verdin J, Shukla S, Husak G, Rowland J, Harrison L, Hoell A, Michaelsen J (2015) The climate hazards infrared precipitation with stations-a new environmental record for monitoring extremes. Sci Data 2:150066, https://doi.org/10.1038/sdata.2015.66, http://www.nature.com/articles/sdata201566, arXiv:10111669v3

Garreaud RD, Vuille M, Compagnucci R, Marengo J (2009) Present-day South American climate. Palaeogeogr Palaeoclimatol Palaeoecol 281(3-4):180–195, https://doi.org/10.1016/j.palaeo.2007.10.032, http://linkinghub.elsevier.com/retrieve/pii/S0031018208005002

Garreaud RD (1999) Cold air incursions over subtropical and tropical South America: a numerical case study. Mon Weather Rev 127(12):2823–2853. https://doi.org/10.1175/1520-0493(1999)127<2823:CAIOSA>2.0.CO;2

Garreaud RD (1999) Multiscale analysis of the summertime precipitation over the central Andes. Mon Weather Rev 127:901–921. https://doi.org/10.1175/1520-0493(1999)127<0901:MAOTSP>2.0.CO;2

Garreaud RD (2000) Cold air incursions over subtropical South America: mean structure and dynamics. Mon Weather Rev 128(7II):2544–2559. https://doi.org/10.1175/1520-0493(2000)128<2544:caioss>2.0.co;2

Garreaud RD (2009) The Andes climate and weather. Adv Geosci 22:3–11. https://doi.org/10.5194/adgeo-22-3-2009

Garreaud RD, Fuenzalida HA (2007) The influence of the Andes on cutoff lows: a modeling study. Mon Weather Rev 135(4):1596–1613. https://doi.org/10.1175/MWR3350.1

Garreaud RD, Wallace JM (1998) Summertime incursions of mid-latitude air into subtropical and tropical South America. Mon Weather Rev 126(10):2713–2733. https://doi.org/10.1175/1520-0493(1998)126<2713:SIOMAI>2.0.CO;2

Garreaud R, Vuille M, Clement AC (2003) The climate of the Altiplano: observed current conditions and mechanisms of past changes. Palaeogeogr Palaeoclimatol Palaeoecol 194(1–3):5–22. https://doi.org/10.1016/S0031-0182(03)00269-4

Gill AE (1980) Some simple solutions for heat-induced tropical circulation. Q J R Meteorol Soc 106(449):447–462. https://doi.org/10.1002/qj.49710644905

Horel JD, Hahmann AN, Geisler JE (1989) An investigation of the annual cycle of convective activity over the Tropical Americas. J Clim 2(11):1388–1403. https://doi.org/10.1175/1520-0442(1989)002<1388:AIOTAC>2.0.CO;2

Hoskins BJ, McIntyre ME, Robertson AW (1985) On the use and significance of isentropic potential vorticity maps. Q J R Meteorol Soc 111(466):877–946. https://doi.org/10.1002/qj.49711146602

Houston J, Hartley AJ (2003) The central Andean west-slope rainshadow and its potential contribution to the origin of hyper-aridity in the Atacama Desert. Int J Climatol 23(12):1453–1464. https://doi.org/10.1002/joc.938

Hunziker S, Gubler S, Calle J, Moreno I, Andrade M, Velarde F, Ticona L, Carrasco G, Castellón Y, Oria C, Croci-Maspoli M, Konzelmann T, Rohrer M, Brönnimann S (2017) Identifying, attributing, and overcoming common data quality issues of manned station observations. Int J Climatol 37(11):4131–4145. https://doi.org/10.1002/joc.5037

Hurley JV, Vuille M, Hardy DR, Burns SJ, Thompson LG (2015) Cold air incursions, δ18O variability, and monsoon dynamics associated with snow days at Quelccaya Ice Cap, Peru. J Geophys Res Atmos 120(15):7467–7487. https://doi.org/10.1002/2015JD023323

Imfeld N, Sedlmeier K, Gubler S, Correa Marrou K, Davila CP, Huerta A, Lavado-Casimiro W, Rohrer M, Scherrer SC, Schwierz C (2021) A combined view on precipitation and temperature climatology and trends in the southern Andes of Peru. Int J Climatol 41(1):679–698. https://doi.org/10.1002/joc.6645

Junquas C, Takahashi K, Condom T, Espinoza JC, Chavez S, Sicart JE, Lebel T (2018) Understanding the influence of orography on the precipitation diurnal cycle and the associated atmospheric processes in the central Andes. Clim Dyn. https://doi.org/10.1007/s00382-017-3858-8

Kasahara A, da Silva Dias PL (1986) Response of planetary waves to stationary tropical heating in a global atmosphere with meridional and vertical shear. J Atmos Sci 43(18):1893–1912. https://doi.org/10.1175/1520-0469(1986)043<1893:ROPWTS>2.0.CO;2

Kiladis GN, Weickmann KM (1992) Circulation anomalies associated with tropical convection during northern winter. https://doi.org/10.1175/1520-0493(1992)120<1900:CAAWTC>2.0.CO;2

Kiladis GN (1998) Observations of Rossby waves linked to convection over the eastern tropical Pacific. J Atmos Sci 55(3):321–339. https://doi.org/10.1175/1520-0469(1998)055<0321:OORWLT>2.0.CO;2

Knippertz P (2007) Tropical-extratropical interactions related to upper-level troughs at low latitudes. Dyn Atmos Ocean 43(1–2):36–62. https://doi.org/10.1016/j.dynatmoce.2006.06.003

Knippertz P, Martin JE (2005) Tropical plumes and extreme precipitation in subtropical and tropical West Africa. Q J R Meteorol Soc 131(610 B):2337–2365. https://doi.org/10.1256/qj.04.148

Lenters JD, Cook KH (1997) On the origin of the Bolivian high and related circulation features of the South American climate. J Atmos Sci 54(5):656–678. https://doi.org/10.1175/1520-0469(1997)054<0656:OTOOTB>2.0.CO;2

Lenters JD, Cook KH (1999) Summertime precipitation variability over South America: role of the large-scale circulation. Mon Weather Rev 127(3):409–431. https://doi.org/10.1175/1520-0493(1999)127<0409:SPVOSA>2.0.CO;2

Marengo J, Cornejo A, Satyamurty P, Nobre C, Sea W (1997) Cold surges in tropical and extratropical south America: the strong event in June 1994. Mon Weather Rev 125(11):2759–2786. https://doi.org/10.1175/1520-0493(1997)125<2759:CSITAE>2.0.CO;2

Mayta VC, Ambrizzi T, Espinoza JC, Silva Dias PL (2019) The role of the Madden-Julian oscillation on the Amazon Basin intraseasonal rainfall variability. Int J Climatol 39(1):343–360. https://doi.org/10.1002/joc.5810

Nacional Sistema, de Defensa Civil P (2006) Plan nacional de contingencia ante la ocurrencia de eventos frios y/o heladas. Tech. rep, SINADECI, Lima

Nie J, Boos WR, Kuang Z (2010) Observational evaluation of a convective quasi-equilibrium view of monsoons. J Clim 23(16):4416–4428. https://doi.org/10.1175/2010JCLI3505.1

Nunes AM, Silva Dias MA, Anselmo EM, Morales CA (2016) Severe convection features in the Amazon basin: a trmm-based 15-year evaluation. Front Earth Sci 4(April):1–14. https://doi.org/10.3389/feart.2016.00037

Paccini L, Espinoza JC, Ronchail J, Segura H (2018) Intra-seasonal rainfall variability in the Amazon basin related to large-scale circulation patterns: a focus on western Amazon-Andes transition region. Int J Climatol 38(5):2386–2399. https://doi.org/10.1002/joc.5341

Parmenter FC (1976) A Southern Hemisphere cold front passage at the equator. Bull Am Meteorol Soc 57(12):1435–1440. https://doi.org/10.1175/1520-0477(1976)057<1435:ASHCFP>2.0.CO;2

Perea-Flores A (2018) El friaje y las heladas: diagnóstico de la problemática en el Perú y legislación comparada. Tech. rep, Departamento de Investigación y Documentación Parlamentaria, Lima

Pinheiro HR, Hodges KI, Gan MA, Ferreira NJ (2017) A new perspective of the climatological features of upper-level cut-off lows in the Southern Hemisphere. Clim Dyn 48(1–2):541–559. https://doi.org/10.1007/s00382-016-3093-8

Poveda G, Espinoza JC, Zuluaga MD, Solman SA, Garreaud R, van Oevelen PJ (2020) High impact weather events in the Andes. Front Earth Sci 8(May):1–32. https://doi.org/10.3389/feart.2020.00162

Satgé F, Ruelland D, Bonnet MP, Molina J, Pillco R (2019) Consistency of satellite-based precipitation products in space and over time compared with gauge observations and snow- hydrological modelling in the Lake Titicaca region. Hydrol Earth Syst Sci 23(1):595–619. https://doi.org/10.5194/hess-23-595-2019

Segura H, Junquas C, Carlo J, Vuille M, Jauregui YR, Rabatel A, Condom T, Lebel T (2019) New insights into the rainfall variability in the tropical Andes on seasonal and interannual time scales. Clim Dyn. https://doi.org/10.1007/s00382-018-4590-8

Segura H, Espinoza JC, Junquas C, Lebel T, Vuille M, Garreaud R (2020) Recent changes in the precipitation-driving processes over the southern tropical Andes/western Amazon. Clim Dyn 54(5–6):2613–2631. https://doi.org/10.1007/s00382-020-05132-6

Seluchi ME, Garreaud R, Fa N, Saulo C (2006) Influence of the subtropical Andes on baroclinic disturbances: a cold front case study. Mon Weather Rev 134(11):3317–3335. https://doi.org/10.1175/MWR3247.1

Sicart JE, Espinoza JC, Quéno L, Medina M (2016) Radiative properties of clouds over a tropical Bolivian glacier: seasonal variations and relationship with regional atmospheric circulation. Int J Climatol 36(8):3116–3128. https://doi.org/10.1002/joc.4540

Silva Dias PL, Schubert WH, DeMaria M (1983) Large-scale response of the tropical atmosphere to transient convection. J Atmos Sci

40(11):2689–2707. https://doi.org/10.1175/1520-0469(1983)040<2689:LSROTT>2.0.CO;2

Sulca J, Takahashi K, Espinoza JC, Vuille M, Lavado-Casimiro W (2018) Impacts of different ENSO flavors and tropical Pacific convection variability (ITCZ, SPCZ) on austral summer rainfall in South America, with a focus on Peru. Int J Climatol 38(1):420–435. https://doi.org/10.1002/joc.5185

Vera CS, Vigliarolo PK (2000) A diagnostic study of cold-air outbreaks over South America. Mon Weather Rev 128(1):3–24. https://doi.org/10.1175/1520-0493(2000)128<0003:ADSOCA>2.0.CO;2

Vera C, Higgins W, Amador J, Ambrizzi T, Garreaud R, Gochis D, Gutzler D, Lettenmaier D, Marengo J, Mechoso CR, Nogues-Paegle J, Silva Dias PL, Zhang C (2006) Toward a unified view of the American monsoon systems. J Clim 19(20):4977–5000. https://doi.org/10.1175/JCLI3896.1

Vuille M (1999) Atmospheric circulation over the Bolivian Altiplano during dry and wet periods and extreme phases of the southern oscillation. Int J Climatol 19:1579–1600. https://doi.org/10.1002/(SICI)1097-0088(19991130)19:14<1579::AID-JOC441>3.0.CO;2-N

Vuille M, Ammann C (1997) Regional snowfall patterns in the high, arid Andes. Clim Change 36(3–4):413–423

Vuille M, Keimig F (2004) Interannual variability of summertime convective cloudiness and precipitation in the central Andes derived from ISCCP-B3 data. J Clim 17:3334–3348. https://doi.org/10.1175/1520-0442(2004)017<3334:IVOSCC>2.0.CO;2

Wang H, Fu R (2002) Cross-equatorial flow and seasonal cycle of precipitation over South America. J Clim 15(13):1591–1608. https://doi.org/10.1175/1520-0442(2002)015<1591:CEFASC>2.0.CO;2

Wang H, Fu R (2004) Influence of cross-Andes flow on the South American low-level jet. J Clim 17(6):1247–1262. https://doi.org/10.1175/1520-0442(2004)017<1247:IOCFOT>2.0.CO;2

Wernli H, Sprenger M (2007) Identification and ERA-15 climatology of potential vorticity streamers and cutoffs near the extratropical tropopause. J Atmos Sci 64(5):1569–1586. https://doi.org/10.1175/JAS3912.1

Zhou J, Lau KM (1998) Does a monsoon climate exist over South America? J Clim 11(5):1020–1040. https://doi.org/10.1175/1520-0442(1998)011<1020:DAMCEO>2.0.CO;2